Chapter 30
Performance of Different Optimization Solvers for Designing Solar Linear Fresnel Reflector Power Generation Systems

M. P. G. Sirimanna, Jonathan D. Nixon, and M. S. Innocente

Abstract Linear Fresnel Reflector (LFR) is an emerging solar thermal power generation technology that benefits from a simple and low-cost construction in comparison to more conventional Concentrating Solar thermal Power (CSP) generation technologies such as parabolic trough and power tower. Although LFR technology presents the drawbacks of lower energy conversion efficiency and higher energy cost, these can be offset by optimizing its design. This has not been sufficiently addressed due to the complex interactions between solar rays, heat transfer modes, and design variables. This work presents a systematic approach to select suitable optimization methods for the design of LFR systems. Thus, a mathematical model is developed to carry out simultaneous raytracing and thermal simulations aiming to provide an estimation of the system's total conversion efficiency to be maximized. In order to compare the performance at solving this problem of a range of optimization algorithms with different characteristics, three derivative-based, two derivative-free, one population-based, and the simulated annealing methods are used in the numerical experiments. Only one design variable and a simple LFR system with a trapezoidal receiver are considered in the first instance. Only those algorithms which are successful at solving this simple problem are then tested on the optimal design with multiple variables. An exhaustive search is also conducted to check accuracy. Results show that pattern search, simulated annealing, and genetic algorithms perform best at solving the simulation-based LFR optimal design problem.

Keywords Concentrating solar thermal power (CSP) · Pattern search · Genetic algorithm · Simulated annealing · Ray-tracing

M. P. G. Sirimanna (✉) · J. D. Nixon
Centre for Fluid and Complex Systems (FCS), Coventry University, Priory Street, Coventry CV1 5FB, UK
e-mail: ae0094@coventry.ac.uk; gayanmrt@gmail.com

M. S. Innocente
Autonomous Vehicles and Artificial Intelligence Laboratory (AVAILAB), Centre for Future Transport and Cities (CFTC), Coventry University, Priory Street, Coventry CV1 5FB, UK

J. D. Nixon et al. (eds.), *Energy and Sustainable Futures: Proceedings of the 3rd ICESF, 2022*, Springer Proceedings in Energy, https://doi.org/10.1007/978-3-031-30960-1_30

30.1 Introduction

With appropriate support, Concentrating Solar thermal Power (CSP) could contribute to 9.6% of global electricity from solar power alone by 2050 [1]. CSP has been developed under four technology categories: Power Tower, Parabolic Trough Collectors, Linear Fresnel Reflector (LFR), and Solar Parabolic Dish. Although LFR has shown potential low energy costs due to its simple design, its annual conversation efficiency is still low (8–10%) compared to the other technologies [2]. Mathematical optimization can be used to improve the efficiency of LFR systems and reduce energy costs, thus making this technology more attractive. In line with this, efficiency improvements to an existing porotype were achieved in 2015 using an analytical design approach [3], although the authors only carried out an optical analysis without optimizing the mirror field design variables. In [4], the geometry of a trapezoidal cavity receiver of an LFR plant was designed to minimise heat loss using ray tracing to simulate heat flux patterns on the receiver tube. However, they did not conduct a detailed analysis of the effect of the mirror field on the receiver. Another optical optimization of the arrangement of LFR mirrors was conducted in [5] considering mirror width, spacing, and focal length. The authors assumed a flat horizontal receiver and suggested including a thermal analysis with a more detailed receiver in future work. Barbón et al. [6] studied the lateral variation of solar energy received on an absorber of small-scale LFR plants. Their main focus was end loss and reflected light loss, which is typically disregarded as they are often negligible in large-scale plants. In 2017, Abbas et al. [7] addressed the optical design of an LFR considering different numbers of mirrors, filling factors, and collector widths. However, the authors made use of a set of predesigns for a solar field without incorporating ray tracing models to reduce the required computational resources facilitating the optimization process. The optimal design of LFR systems making use of coupled optical ray-tracing and thermal models and considering both mirror field and receiver design parameters simultaneously has not been sufficiently investigated. The aim of this study is to identify a suitable optimization method which can solve this challenging problem.

30.2 Methodology

A mathematical model is developed by combining energy balance, ray tracing, and thermal modelling. The objective function for the LFR optimal design is given by the total theoretical efficiency ($\eta_{total,th}$) assuming a coupled Carnot cycle [8, 9]. The design variables are the number of mirrors (n_m), mirror width (w_m), mirror spacing (s_m), receiver height (h_r), and receiver width (w_r).

Seven optimization methods with different characteristics are tested to investigate their efficiency, as well as their different trade-offs between accuracy and required computational effort. Namely, interior-point (IP), sequential quadratic programming

(SQP) and active-set (AS) methods are derivative-based; pattern search (PS), Nelder-Mead simplex (NMS) and simulated annealing (SA) methods are derivative-free; whilst genetic algorithm (GA) is both a derivative-free and population-based method. This particular choice of methods is based on the literature and on their availability within Matlab's optimization toolbox.

The optimization problem is initially reduced to a single design variable, namely the receiver height. The problem is then solved using the PS, NMS, SA and GA methods. The worst-performing algorithm is eliminated (NMS, referred to as fminsearch in Matlab), and the other three are tested on the original five-dimensional optimization problem discussed before. It is fair to note that the number of mirrors (n_m) is a discrete variable. In order to avoid a mixed-discrete problem, a four-dimensional continuous problem is solved instead for each of a few selected values of n_m.

30.3 Models

Based on the conservation of energy principle, the energy output of the LFR system (Q_o) can be found from the difference between the heat input (Q_{in}) to the receiver and the heat loss to ambient air (Q_{loss}) [10].

$$Q_o = Q_{in} - Q_{loss} \tag{30.1}$$

After reflection on the mirrors, the solar energy incident over the receiver area, A_r, is absorbed by the working fluid as heat, increasing the receiver temperature (T_r). The absorbed solar energy becomes the heat input to the system (Q_{in}). A portion of absorbed energy is lost to the surrounding, which is at temperature T_a. The heat output of an LFR system can therefore be described by [11, 12]

$$Q_o = I_{r,abs} A_r - A_r U_L (T_r - T_a) \tag{30.2}$$

where $I_{r,abs}$ and U_L are absorbed solar radiation and heat loss coefficient of the receiver.

There are analytical methods and numerical approaches to calculate $I_{r,abs}$ for different LFR systems. SolTrace tool has been used in this study considering its ability to model complex geometries with good accuracy [13]. U_L is calculated using analytical and empirical correlations considering conduction, convection and radiation losses of the receiver [11, 14].

If solar energy received on the effective aperture of all mirror elements is E_m, the total theoretical efficiency ($\eta_{total,th}$) can be obtained as in Eq. (30.3), assuming coupled Carnot cycle [8, 9].

$$\eta_{total,th} = \frac{Q_o\left(1 - \frac{T_a}{T_r}\right)}{E_m} \tag{30.3}$$

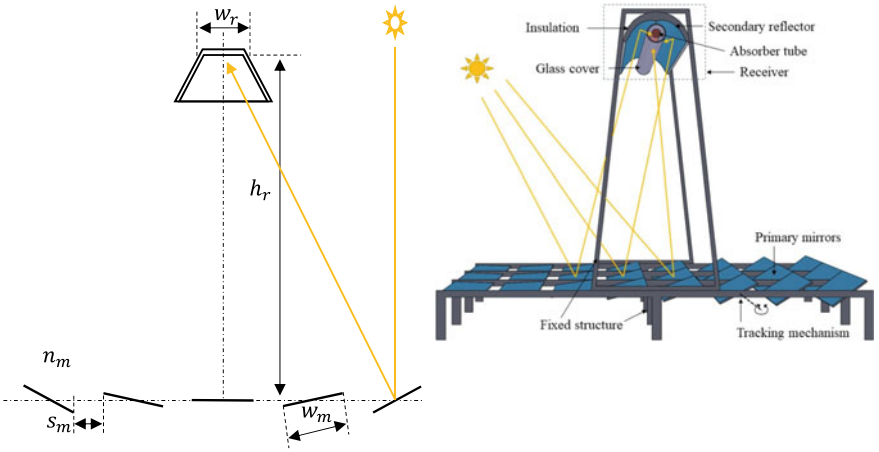

Fig. 30.1 **a** Schematic of a 2D view of an LFR system with a trapezoidal cavity receiver, **b** a schematic diagram of a typical LFR system

The objective function to be optimized is $\eta_{total,th}$ and the design variables are the number of mirrors (n_m), mirror width (w_m), mirror spacing (s_m), receiver height (h_r) and receiver width (w_r), as shown in Fig. 30.1.

30.4 Results and Discussion

30.4.1 Candidate Derivative-Free and Population-Based Methods

Two derivative-free methods, pattern search and fminsearch solver in Matlab, were selected and eight simulations were carried out for each method. Figure 30.2a shows that all eight optimization results are gathered around the neighbourhood of the global optimum. These results show a very good agreement with the exhaustive search. Two global optimization methods, Simulated Annealing and GA, were also used to check their behaviour for the objective function. Five simulations were run for Simulated Annealing and three simulations were run for GA. As seen in Fig. 30.2b, all these results lay between 22 and 23 and were very close to the global optimum, $h_r = 23$. All simulations were run using default settings except the function tolerance, which was reduced to 10^{-3} to minimise the effect of numerical disturbance of the model. It is seen that simulated annealing and GA have shown the best results in consecutive runs showing close solutions to each other.

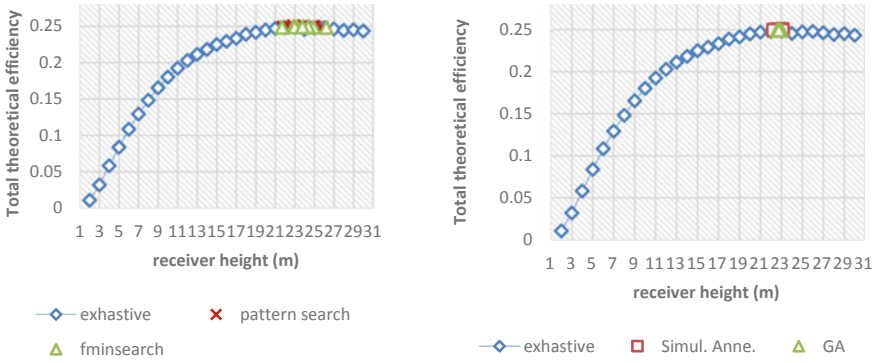

(a) (b)

Fig. 30.2 **a** Comparison of exhaustive search results against two derivative-free methods **b** against a population-based method (GA) and simulated annealing

30.4.2 A Candidate Optimization Method for a Multidimensional Problem

Optimization was expanded to four continuous variables (w_m, s_m, h_r, w_r) while keeping the fifth one (n_m) at a few selected discrete values. Thus a four-dimensional continuous optimization problem is solved for each value of n_m. Only the PS, SA and GA algorithms are tested here, which are the ones which performed best in the one-dimensional problem. In order to assess the accuracy of the optimizers, an exhaustive search was performed discretizing all four continuous variables (see Table 30.1).

The ten best simulation results from the exhaustive search for $n_m = 10$ are shown in Table 30.2. It can be observed that the differences between the efficiency of the global optimum and that of neighbouring designs are very small. In fact, the first two solutions may be deemed global maxima if rounding efficiency to three decimals. Then, the global maxima would be found at $h_r = 9$ m, $w_r = 0.9$ m, $w_m = 0.9$

Table 30.1 Design variables and their discretization for exhaustive search

Variable	Range	Discretization for exhaustive search	
		Step size	Sample values
Receiver height (h_r)	$1 \leq h_r \leq 30$	4 m	1, 5, 9, …, 21, 25, 29
Mirror width (w_m)	$0.1 \leq w_m \leq 1.2$	0.2 m	0.1, 0.3, 0.5, …, 0.9, 1.1
Mirror spacing (s_m)	$0.05 \leq s_m \leq 0.3$	0.05 m	0.05, 0.1, 0.15, …, 0.25, 0.3
Receiver width (w_r)	$0.1 \leq w_r \leq 1.2$	0.2 m	0.1, 0.3, 0.5, …, 0.9, 1.1
Number of mirrors (n_m)	$2 \leq n_m \leq 78$	4	2, 6, 10, …, 74, 78

m, whilst s_m could take either 0.09 m or 0.13 m. However, the design variables are discretised. For the continuous case, the actual global optimum may lie nearby. Therefore, it is possible that a global search algorithm is able to find even better solutions than this so-called exhaustive search.

The optimal designs returned by PS, SA and GA are shown in Table 30.3. It is seen that all solvers achieve a maximum $\eta_{total,th}$ between 0.170 and 0.172 (i.e. 17–17.2%). Figure 30.3 shows a comparison of these results in terms of the maximised solution.

Table 30.2 Results of the exhaustive search for $n_m = 10$

h_r (m)	w_r (m)	w_m (m)	s_m (m)	Max $\eta_{total,th}$	Max $\eta_{total,th}$ rounded
9	0.9	0.9	0.09	0.169046	0.169
9	0.9	0.9	0.13	0.168863	0.169
13	0.9	0.9	0.29	0.168355	0.168
13	0.9	0.9	0.17	0.168300	0.168
13	0.9	0.9	0.25	0.167729	0.168
9	0.9	0.9	0.05	0.167573	0.168
13	0.9	0.9	0.21	0.167472	0.167
9	0.9	0.9	0.17	0.167419	0.167
13	0.9	0.9	0.09	0.167098	0.167
13	0.9	0.9	0.05	0.166906	0.167

Table 30.3 Optimization results of three optimization algorithms for $n_m = 10$

Number of mirrors (n_m) = 10		Pattern search		Simulated annealing		Genetic algorithm	
		Optimal design (m)	Max $\eta_{total,th}$	Optimal design (m)	Max $\eta_{total,th}$	Optimal design (m)	Max $\eta_{total,th}$
1st run	h_r	10.5	0.1713	9.92	0.1715	8.92	0.1711
	w_r	0.878		0.852		0.799	
	w_m	0.89		0.861		0.833	
	s_m	0.247		0.103		0.115	
2nd run	h_r	11	0.1701	9.9	0.1703	10.276	0.1715
	w_r	0.8		0.867		0.867	
	w_m	0.89		0.889		0.885	
	s_m	0.285		0.076		0.157	
3rd run	h_r	10	0.1717	8.738	0.1697	9.86	0.1719
	w_r	0.878		0.81		0.873	
	w_m	0.89		0.788		0.902	
	s_m	0.193		0.166		0.177	

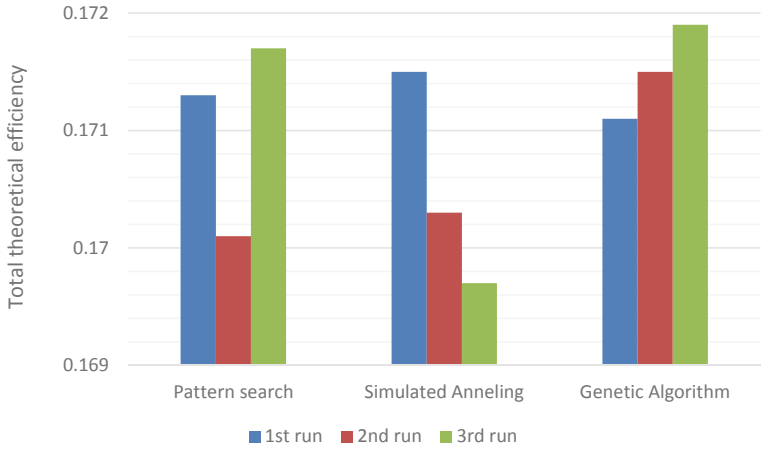

Fig. 30.3 Comparison of maximised $\eta_{total,th}$ using three optimization algorithms ($n_m = 10$)

The same process of comparing the exhaustive search and optimal solutions was repeated for $n_m = 30$ and $n_m = 54$. Results show a similar behaviour to $n_m = 10$, where an optimal solution was found within the same region of the search-space as the exhaustive search. Although the three optimization algorithms found better solutions, it should be noted that the discretization of continuous search space has greatly affected these results. A comparison of the results of these two different simulations is shown in Fig. 30.4. The average simulation times for the three algorithms are shown in Fig. 30.5.

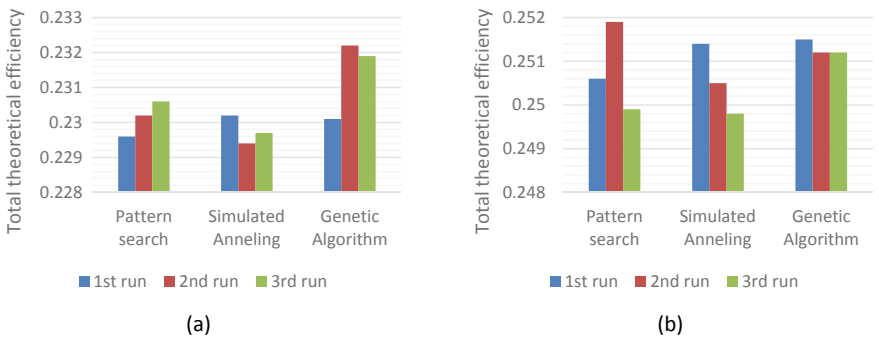

Fig. 30.4 A comparison of three optimization algorithms: **a** $n_m = 30$; **b** $n_m = 54$

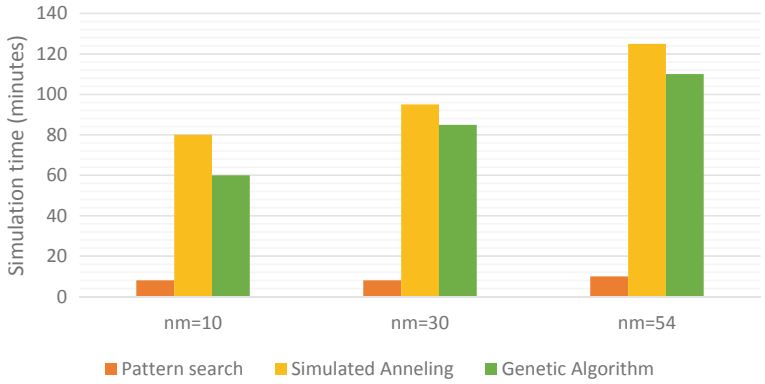

Fig. 30.5 Average simulation time for all three optimization algorithms

30.5 Conclusion

After considering all the simulation results, it is seen that pattern search, simulated annealing and genetic algorithm provided acceptable solutions. The differences between the best and the worst solutions using pattern search, simulated annealing and GA were 0.0012–0.0020, 0.0008–0.0018 and 0.0003–0.0020 respectively. The largest difference found was 0.002, equal to 0.2% of the total theoretical efficiency, which is more than enough for many practical applications. Since all algorithms provided acceptable results, the selection of an algorithm for further work can be decided based on the simulation time and the ease of handling the discrete design variable, number of mirrors, within the optimization codes.

It is clearly seen that the pattern search is 8–10 times faster than the other two algorithms in terms of computational time. Increasing the simulation time for larger mirror numbers is also significantly lower in comparison. The genetic algorithm seems to be slightly better than simulated annealing taking 10–20 min less simulation time. However, it is important to note that for population-based methods like GA, the initial setup is usually time consuming and adding extra variables is relatively easy.

References

1. IRENA, *Technology Roadmap, Concentrating Solar Power* (International Energy Agency, 2010)
2. M.T. Islam et al., A comprehensive review of state-of-the-art concentrating solar power (CSP) technologies: current status and research trends. Renew. Sustain. Energy Rev. **91**, 987–1018 (2018), Available at: http://www.sciencedirect.com/science/article/pii/S1364032118303113. https://doi.org/10.1016/j.rser.2018.04.097
3. R. Abbas, J.M. Martínez-Val, Analytic optical design of linear Fresnel collectors with

variable widths and shifts of mirrors. Renew. Energy **75**, 81–92 (2015), Available at: http://www.sciencedirect.com/science/article/pii/S0960148114005941. https://doi.org/10.1016/j.renene.2014.09.029
4. M.A. Moghimi, K.J. Craig, J.P. Meyer, Optimization of a trapezoidal cavity absorber for the Linear Fresnel Reflector. Solar Energy **119**, 343–361 (2015), Available at: http://www.sciencedirect.com/science/article/pii/S0038092X15003771. https://doi.org/10.1016/j.solener.2015.07.009
5. P. Boito, R. Grena, Optimization of the geometry of Fresnel linear collectors. Solar Energy **135**, 479–486 (2016), Available at: http://www.sciencedirect.com/science/article/pii/S0038092X16301785. https://doi.org/10.1016/j.solener.2016.05.060
6. A. Barbón et al., Optimization of the length and position of the absorber tube in small-scale Linear Fresnel Concentrators. Renew. Energy **99**, 986–995 (2016), Available at: http://www.sciencedirect.com/science/article/pii/S0960148116306851. https://doi.org/10.1016/j.renene.2016.07.070
7. R. Abbas et al., Design of an innovative linear Fresnel collector by means of optical performance optimization: a comparison with parabolic trough collectors for different latitudes. Solar Energy **153**, 459–470 (2017), Available at: http://www.sciencedirect.com/science/article/pii/S0038092X17304255. https://doi.org/10.1016/j.solener.2017.05.047
8. M. Romero, J. Gonzalez-Aguilar, E. Zarza, Concentrating solar thermal power, in *Energy Efficiency and Renewable Energy Handbook*, 2nd edn., ed. by D.Y. Goswami, F. Kreith (CRC Press, Boca Raton, 2015), pp.1237–1246
9. J.D. Nixon, P.A. Davies, Cost-exergy optimisation of linear Fresnel reflectors. Solar Energy **86**(1), 147–156 (2012), Available at: http://www.sciencedirect.com/science/article/pii/S0038092X11003501. https://doi.org/10.1016/j.solener.2011.09.024
10. G. Morin et al., Comparison of linear Fresnel and parabolic trough collector power plants. Solar Energy **86**(1), 1–12 (2012), Available at: https://www.sciencedirect.com/science/article/pii/S0038092X11002325. https://doi.org/10.1016/j.solener.2011.06.020
11. J.A. Duffie, W.A. Beckman, *Solar Engineering of Thermal Processes*, 4th edn. (Wiley, New Jersey, 2013)
12. H. Zheng, Chapter 2—solar energy utilization and its collection devices, in *Solar Energy Desalination Technology*, ed. by H. Zheng (2017), Available at: https://www.sciencedirect.com/science/article/pii/B9780128054116000026. https://doi.org/10.1016/B978-0-12-805411-6.00002-6
13. T. Wendelin, A. Dobos, A. Lewandowski, *SolTrace: A Ray-Tracing Code for Complex Solar Optical Systems* (United States, 2013)
14. R. Forristall, *Heat Transfer Analysis and Modeling of a Parabolic Trough Solar Receiver Implemented in Engineering Equation Solver* (US Department of Energy (US), United States, 2003), Available at: http://www.osti.gov/scitech/biblio/15004820. https://doi.org/10.2172/15004820